Post-Disaster Building Damage Assessment Using 3D Surface Models Derived from Unmanned Aerial Vehicle (UAV) Imagery

Alyssa Patricia J. Manzano[1] and Ariel C. Blanco[1,2]

[1]Department of Geodetic Engineering, University of the Philippines Diliman, Quezon City, Philippines – ajmanzano@up.edu.ph
[2]Training Center for Applied Geodesy and Photogrammetry, University of the Philippines Diliman, Quezon City, Philippines – acblanco@up.edu.ph

Keywords: Structure-from-Motion (SfM), Texture Analysis, Topographic Modeling, Correlation-Based Feature Selection, Random Forest

Abstract

The Philippines is highly vulnerable to tropical cyclones (TCs), which frequently cause devastating impacts on infrastructure and communities. Rapid and accurate identification of damage extent and location is essential to trigger appropriate post-disaster response, expedite recovery, and facilitate better reconstruction. This study developed a methodology to classify building damage using unmanned aerial vehicle (UAV) images collected in February 2014 after Typhoon Haiyan hit the study area located in Tacloban City in November 2013. The methodology employed Structure-from-Motion (SfM) technique, texture analysis, and topographic modeling to analyze and extract building damage information. A damage rating system using percent area of damage as basis for damage severity was also developed. Correlation-based feature selection algorithm was used to refine and reduce the possible building damage predictor attributes. Random Forest was used to predict each building's level of damage. Binary model R-A1, which classified completely damaged and undamaged buildings, had an accuracy of 93.5%, average precision of 0.938, average recall of 0.935 and average f-measure of 0.935, while model R-A2, which classified damaged and undamaged buildings, had an accuracy of 80.3%, average precision of 0.803, average recall of 0.803 and average f-measure of 0.803. Ternary model R-B1, which classified completely damaged, partially damaged and undamaged buildings, had an accuracy of 81.6%, average precision of 0.812, average recall of 0.816, and average f-measure of 0.813. The R-A2 model had an accuracy of 73.4% when tasked to classify 613 previously unseen damaged buildings. The R-B1 model had an accuracy of 70.3% when tasked to classify 575 previously unseen partially damaged and completely damaged buildings. This study highlighted the challenges in identifying and classifying building damage markers, some of which are unique to the Philippine setting, and demonstrated the value of UAV-based assessments for rapid and high-resolution damage evaluation.

1. Introduction

1.1 Background

The Philippines faces frequent and severe impacts from typhoons, including extreme winds, heavy rains, and storm surges. Super Typhoon Haiyan (Yolanda) underscored the urgent need for efficient post-disaster damage assessment, with huge infrastructure losses and slow recovery due to delays in assessing the extent of destruction. Tacloban City suffered infrastructure damage worth almost Php 2.5B, with 12,270 totally damaged houses and 46,553 partially damaged houses (NDRRMC, 2014).

Efficient damage assessment is vital for effective post-disaster recovery, guiding early relief efforts, resource allocation, and long-term reconstruction. Traditional methods such as ground surveys for post-disaster assessment, while reliable, are often slow, labor-intensive and risky (Cao & Choe, 2020), thus delaying critical aid delivery. In the case of Tacloban City, the government took 16 to 18 months after Super Typhoon Haiyan hit to distribute cash aid mainly due to the lack of data such as names and category of shelter damage since government agencies relied mostly on ground reports submitted by LGUs (Perante, 2016). Remote sensing, particularly the use of unmanned aerial vehicles (UAVs), has emerged as a promising tool to bridge gaps in traditional assessment methods. UAVs can capture high-resolution imagery over extensive areas quickly and cost-effectively, even in hazardous conditions, enabling timely analyses and actionable insights (Everaerts and V, 2008; Mathews et al., 2023).
This study explored the use of UAV imagery combined with remote sensing techniques, such as Structure-from-Motion processing, topographic modeling, and texture analysis, as well as machine learning classifiers like Random Forest, to map building damage after Typhoon Haiyan. This study developed a remote sensing-based damage rating system, which used the percent area of damage as basis for the damage rating. This study identified building and roof damage indicators, and used those damage indicators to classify buildings according to damage severity. This study also evaluated the sensitivity of the model by comparing results of binary (undamaged versus damaged, and undamaged versus completely damaged) and ternary (undamaged, partially damaged and completely damaged) classes, as well as datasets using original and resampled orthomosaic, DSM and DTM resolutions. By improving the speed and accuracy of damage assessment, UAV-based approaches can better support timely aid distribution and resilient rebuilding efforts.

1.2 Study Area

The study area is located within Tacloban City and has a total land area of 245,999 square meters. It includes parts of Barangays 53, 54, 54-A, El Reposo (55, 55-A), 56, and 56-A. Barangays 54-A and 56-A are along the coastline facing Cancabato Bay (Figure1).

[1] This paper is based on the first author's Master's thesis "Post-disaster infrastructure damage assessment using 3D surface models derived from unmanned aerial vehicle (UAV) imagery", University of the Philippines Diliman, 2025.

https://doi.org/10.5194/isprs-annals-X-5-W4-2025-331-2026 | © Author(s) 2026. CC BY 4.0 License.

Due to its proximity to Cancabato Bay, the study area was affected by the massive storm surge that was caused by Typhoon Haiyan. The buildings observed inside the study area were found to be varied in terms of construction materials used, as well as in terms of roof types, height and designs. The buildings also exhibited different levels or severity of damage, with various types of post-typhoon damage indicators available. These settings and conditions make the study area a good representation of a post-typhoon devastated site with mixed infrastructure types commonly found in the Philippines.

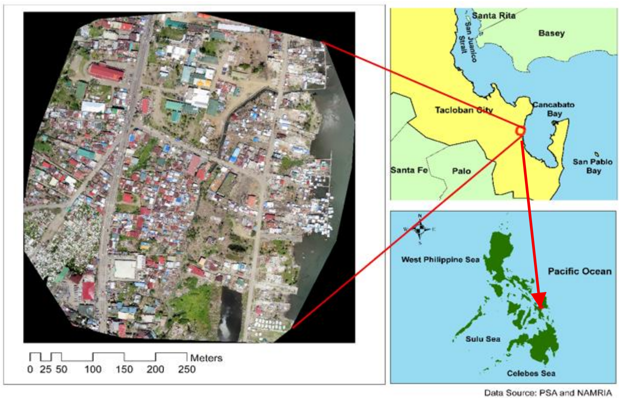

Figure 1. Orthomosaic of study area located in the southeastern part of Tacloban City near Cancabato Bay. Inset maps show location of study area (in red) in Tacloban City and the Philippines.

1.3 Data Sources

The UAV images used in this study were acquired by SkyEye Analytics, Inc., which deployed a custom-built fixed-wing UAV equipped with a Canon PowerShot S100 camera to capture aerial photographs of Tacloban City. The photos were taken on the 19th of February in 2014, three months after Typhoon Haiyan's landfall in Tacloban City. Due to data availability constraints, this was the earliest UAV imagery accessible to the proponents, which represents a limitation of the study. During this period, debris clearing, temporary repairs, and vegetation regrowth may have reduced the visibility of certain damage indicators, particularly for moderate damage, which could lead to underestimation. However, severe roof loss and structural collapse remained clearly identifiable. The deployment produced 463 images for the northern part of Tacloban City but in order to limit processing cost, only 123 images were used for this study.

2. Related Work

Studies focused on remote sensing-based building damage assessment employed various methods and different damage markers to identify and classify building damage. Object-based classification, pattern recognition, template matching and supervised classification are techniques used to get damage information (Joshi et al., 2017). Change detection, which requires pre- and post-disaster event images, is a popular method to get building damage information (Dong & Shan, 2013). However, several studies are now focusing on using only post-disaster event data as it is a reality that sometimes pre-disaster event data are not available.

Building geometry, spectra and texture feature information can be used as building damage markers for remote sensing-based damage assessment. Sonobe (2020), Akhmadiya et al. (2022), and Joshi et al. (2017) focused on texture features as damage indicators. A mix of texture and geometric features as damage indicators were explored by Tu et al. (2016) and Cooner et al. (2016). Miura et al. (2020) and Gonsoroski et al. (2023) included the presence of blue tarpaulins as a damage indicator.

Studies that focused on neighborhood spatial scale using UAV images tend to not include the damage to facades. They typically included only the roof areas and considered the degree of structural collapse. Yeom et al. (2019) used elevation and spectral difference to detect intact building regions after a hurricane event. Wen et al. (2023) used spectral, texture, and geometric features derived from post-earthquake UAV data. Due to the number of damage indicators considered, a machine learning technique called recursive feature elimination (RFE) was employed.

As of writing, there is no standardized remote sensing-based damage scale for buildings affected by typhoon. Studies included in the review have used their own damage scales and criteria. There is still a challenge in determining intermediate damage states when using image-based techniques (Kerle et al., 2020). Womble (2005) proposed a remote sensing-based damage scale which only relied on vertical views of buildings. However, the physical damage indicators such as removed shingles and tiles cannot be used for buildings found in the Philippines.

The approaches discussed in the review were primarily developed for building types and materials in other regions and may not accurately capture the specific damage patterns seen in Philippine structures. Research indicates that classification models often underperform when processing unfamiliar or untrained data (Vetrivel et al., 2015), highlighting the need to study and characterize damage indicators typically observed in post-typhoon settings in the Philippines.

3. Methodology

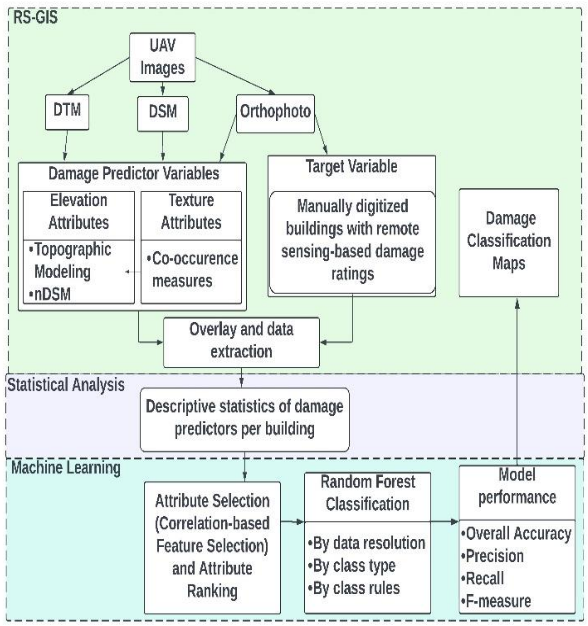

Figure 2. Conceptual framework of the study integrating remote sensing, GIS, statistical analysis, and machine learning to identify and utilize building damage markers for automated damage classification.

Figure 2 shows the conceptual framework of the study. This study involves the use of remote sensing, GIS, statistical analysis and machine learning concepts to achieve the research objectives. The main goal is to identify building damage markers, and then transform these remotely-sensed damage markers into machine-understandable information that would then allow automatic damage classification of buildings.

3.1 Damage Rating System

The damage rating system developed and used in this study is remote sensing-based. Remote sensing data, in this case UAV data, is often limited to top or vertical view and does not include the façades of buildings. This building damage rating system uses percent damaged area (PDA) to rate building damage. The PDA is determined by visually estimating the damaged area as a proportion of total top view area of the building. The damaged area is an area on the building that visually contains any of the physical damage indicators. Damage indicators include any markers and proxies that represent damage to buildings. For this study, the physical damage indicators were vegetation or collapsed trees, rips, folds, warps, holes, changes in roof color, tarpaulins, debris, collapsed building parts, and exposed roof parts. The PDA was then used as the basis for the damage rating (DR) and for formulating the binary and ternary classification rules detailed in Appendix Table A1. Figure 3 shows a building with DR of 2.

Figure 3. Building with damage rating of 2. Yellow arrows show the damage indicators. Damaged area is approximately less than 20 percent of the total building polygon's area.

3.2 Generation of DSM, DTM and Orthomosaic

Structure-from-Motion (SfM) was employed using Pix4D to generate the orthophotos, Digital Surface Models (DSM), and Digital Terrain Models (DTM). The DSM and orthomosiac had a resolution of 4.76 cm while the DTM had a resolution of 23.88 cm. The original resolution dataset was sourced from these images. Lower resolution images were then produced using ArcGIS' Resample tool. The resampled orthomosaic and DSM have a resolution of 9.55 cm, while the resampled DTM has a resolution of 47.76 cm. The resampled resolution dataset was sourced from these images.

3.3 Generation of Attributes

Original and resampled resolution DTM, DSM, and orthomosaic were used as inputs to produce nDSM, topographic modeling and texture information of the buildings. Two main types of attributes were used as predictor variables of classification models: elevation attribute and texture attribute.

3.3.1 Elevation Attributes. In ArcGIS, the Raster Calculator tool was used to generate the normalized DSM (nDSM). The nDSM is calculated by subtracting the DTM from DSM. This represents the relative height of objects above the surrounding ground surface.

For this study, topographic models were used to study the surfaces of roofs and remnants of damaged buildings. The produced DSM was loaded to ENVI (version 4.8) in order to run its Topographic Modeling tool. The default topographic kernel size of 3 was used.

3.3.2 Texture Attributes. For this study, the second-order occurrence filters were produced to generate texture metrics data. ENVI's Co-occurrence Measures tool was used to produce the mean, variance, homogeneity, contrast, dissimilarity, entropy, second moment, and correlation filters for the hue, saturation and value orthomosaic images.

3.3.3 Descriptive Statistics of Attribute Data. The digitized building layer was overlaid on the candidate attribute layer in ArcGIS. The Extract Values to Table tool was then used to extract the pixel values of the candidate attribute contained in one building. XLSTAT, a statistical software add-on for Excel, was then used to compute descriptive statistics of each candidate attribute for each building.

3.4 Feature Selection

WEKA's CfsSubsetEval algorithm was used in order to reduce the number of features being considered. This correlation-based feature selection algorithm is used to evaluate the worth of a subset of attributes by considering the degree of redundancy between each feature and the individual predictive ability of each feature (Hall, 2000). Irrelevant and redundant features are ignored by this multivariate method (Arun Kumar et al., 2017). The algorithm was applied to binary (A1), ternary (B1) and 11-class (DR) original resolution datasets described in Table A1.

3.5 Classification Using Random Forest

The Random Forest algorithm in WEKA was used for classification. Cross-validation (10-folds) was again used to evaluate the classification model. The complexity of having numerous attributes demand a high number of instances to train the model. Cross-validation eliminates the need to divide the data into test and train groups. In order to avoid an imbalanced dataset, undersampling method was used to balance the datasets except for the one used by the A1 models, which only included undamaged and completely damaged buildings. Using Random Forest's "Attribute Ranking" function, features were further reduced until there was no more improvement in model performance. Random Forest models' accuracy, precision, recall and f-measure were then evaluated in order to select the best binary and ternary class models. The buildings that were not used in training the model were classified by running the "Re-evaluate model on current test set" option on WEKA. This approach applies the best-performing model to the entire dataset, thus allowing for the classification of all buildings and the subsequent generation of building damage maps.

4. Results and Discussion

4.1 Digitized Buildings with Assigned Damage Ratings

A total of 689 digitized buildings were used in this study. The remote sensing-based damage rating system was found to be fairly easy to use and can be flexible enough to be used in other areas affected by disaster. Proponents can define damage indicators that can be seen in their affected area and use the percent damage area covered by those damage indicators to determine the damage ratings of buildings. The method is thus more objective and readily quantitative since it does not rely on the presence of specific physical damage indicators that may not be applicable to certain environments or buildings. Just like with other damage assessment studies that only used vertical view data, this damage rating system did not include walls, windows and doors. This rating system also did not include water or flood damage. These are limitations of remote sensing-based data, and are tradeoffs of accomplishing a rapid damage assessment.

4.2 Selected Features

A total of 16 predictor attributes were used for the models in this study. The elevation attributes are nDSM, aspect and slope. The texture attributes are hue-dissimilarity, hue-entropy, hue-homogeneity, hue-mean, hue-second moment, saturation-correlation, saturation-mean, value-contrast, value-correlation, value-dissimilarity, value-entropy, value-second moment, and value-variance. The number of features for the optimized models are shown in Table 1.

Model Name	Attributes	No. of Features	No. of Buildings
O/R-A1-e	Elevation only	4	93
O/R-A1-t	Texture only	17	
O/R-A1	All	21	
O/R-A2	All	25	76
O/R-A3	All		405
O/R-B1-e	Elevation only	18	114
O/R-B1-t	Texture only	65	
O/R-B1	All	83	
O/R-B2	All		351

Table 1. Different classification models produced with the corresponding no. of features and no. of buildings used.

4.3 Random Forest Classification

All the models that used the resampled (lower) resolution dataset consistently outperformed the models that used the original (higher) resolution dataset. Elevation attributes performed best when using original or higher resolution dataset, while texture attributes performed best when used with resampled or lower resolution datasets A possible explanation is that higher resolution data captured fine-scale variations unrelated to structural damage, such as roof surface heterogeneity, shadows, reflections, and photogrammetric artifacts. Downsampling could have smoothed these variations thus reducing noise in texture metrics and making predictors more representative of actual damage patterns. In contrast, higher resolution datasets may have performed better in some models when using only elevation attributes, as the finer detail preserved subtle height changes, roof warping, and sharp edge features that are diminished when resampled. When texture and elevation attributes were used together, the lower resolution datasets yielded better results likely because texture attributes, which outnumbered elevation attributes and were more sensitive to noise, influenced the model more strongly. The lower resolution data reduced noise in the texture attributes while preserving enough detail in the elevation attributes for them to remain useful in the classification.

Based on attribute ranking scores, hue-based measures (e.g. hue-dissimilarity, entropy and homogeneity) were found to be critical for both resolutions, and for all models. A1 models that used texture attributes only performed better than those that used elevation attributes only, but performed best when both attribute types are used together. For both O-A2 and R-A2, minimum nDSM and slope variation coefficient had the highest importance among all features. For the B1 models, using elevation attributes only performed better when using the original resolution dataset, but when using texture attributes only, the model performed better with resampled resolution dataset. Table 2 shows the comparison of results between the different binary and ternary class models.

Model Name	Accuracy (%)	Ave. Precision	Ave. Recall	Ave. F-measure
O-A1-e	86.0	0.861	0.860	0.860
R-A1-e	82.8	0.830	0.828	0.829
O-A1-t	89.2	0.892	0.892	0.892
R-A1-t	93.5	0.938	0.935	0.935
O-A1	93.5	0.935	0.935	0.935
R-A1	**93.5**	**0.938**	**0.935**	**0.935**
O-A2	78.9	0.789	0.789	0.789
R-A2	**80.3**	**0.803**	**0.803**	**0.803**
O-A3	70.8	0.708	0.708	0.708
R-A3	71.2	0.712	0.712	0.712
O-B1-e	68.4	0.675	0.684	0.672
R-B1-e	64.9	0.641	0.649	0.643
O-B1-t	62.3	0.621	0.623	0.622
R-B1-t	73.7	0.732	0.737	0.733
O-B1	69.3	0.692	0.693	0.692
R-B1	**81.6**	**0.812**	**0.816**	**0.813**
O-B2	57.3	0.573	0.573	0.573
R-B2	60.4	0.609	0.604	0.606

Table 2. Classification performance metrics of binary and ternary class models. The models with the best performance metrics are in red bold font.

4.4 Misclassified Buildings

The buildings with roofs made of corrugated metal sheets (Figure 4) were often misclassified as damaged by models using high resolution datasets. Undamaged roofs with homogenous color were classified correctly, but those that had rusted corrugated sheets were most often misclassified as damaged. The misclassification was because of the texture attributes since models that used elevation only attributes rarely made the same mistake. Although some buildings with corrugated metal roof sheets were correctly classified, the results show there is a need for more samples with this type of roof in order to improve classification performance. Many buildings were found to have this type of roofing material, often overlapping with one another, which led to difficulty in both digitization and damage rating assignment.

Figure 4. Building with roof made of rusted corrugated sheets. The rusted and uneven texture of the roofing material introduced noise in the texture attributes, leading to frequent misclassification as damaged despite being intact.

Models that used elevation attributes only had difficulty in correctly classifying buildings with exposed roof beams. This might be due to the fairly low resolution of the nDSM image, and because A1 and A2 models only considered the minimum value of nDSM. Buildings with very low minimum nDSM values tend to be classified as damaged. The building in Figure 5 however, had high minimum nDSM due to the resolution. The spaces between the roof beams cannot adequately be seen using the nDSM image. Such buildings were correctly classified when texture and elevation attributes were used together.

Figure 5. Building with exposed roof beams. These features can cause misclassification in elevation-only models due to limited nDSM resolution.

The models often misclassified buildings with DR 1 as undamaged. Some roof damage may be considered as negligible; however, the damage rating rules were strictly followed. Meanwhile, some highly, but only partially damaged, buildings were misclassified as completely damaged. It was seen that some buildings had pieces of wood, tarpaulin or corrugated metal roof sheets as temporary repairs of the damaged parts. The change in texture and color tend to be identified as damage by the models. Some buildings, especially those with PDA of 70% to 90% had to be labelled partially damaged following the damage rating rules of this study but can already be considered unlivable or completely damaged.

Often, when models using texture attributes only are wrong and models using elevation attributes only are correct, models using both attributes would result to a wrong classification. Figure 6 shows a building that was misclassified by O-B1-t as partially damaged, but correctly classified by O-B1-e as completely damaged. Only some walls and floor fixtures are left. Using both texture and elevation attributes still resulted in a misclassification.

Figure 6. Completely damaged building misclassified as partially damaged. Although elevation attributes correctly classified it, using texture attributes led to misclassification due to conflicting cues.

Some undamaged buildings with smooth roof surfaces were also found to have aspect images that exhibited uneven surfaces (Figure 7). Despite the absence of physical damage, these aspect images revealed irregular patterns that suggested surface variation, which contributed to their misclassification as damaged buildings. This occurs because extracting elevation data from homogenous or patternless surfaces like smooth roofs is extremely difficult. Such areas often lack distinguishable features needed for accurate image matching or point cloud generation, resulting in higher positional errors and the appearance of artificial surface irregularities in derived products like aspect images.

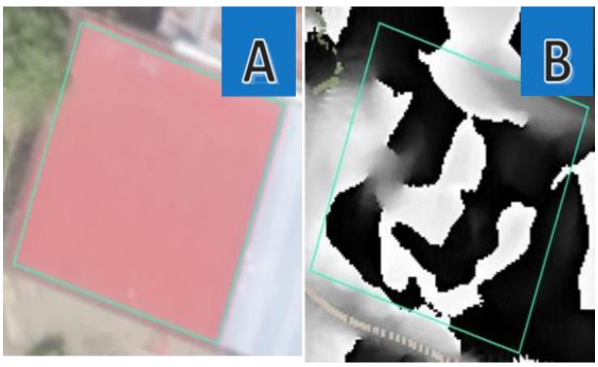

Figure 7. Building with smooth roof texture. (a) Orthophoto image and (b) aspect image.

5. Conclusions and Recommendations

This study developed a methodology to classify buildings based on damage severity levels using UAV data collected after a typhoon. The remote sensing-based damage rating system, which utilizes the percentage of damaged area, offers a relatively more objective and readily quantifiable approach, making it straightforward and easy to use. However, since the percentage of damaged area was visually estimated, the process still involves certain degree of subjectivity. Using semi-automated or automated extraction methods in future work could help reduce this subjectivity and improve reproducibility.

Roof and building damage indicators were extracted using the nDSM, topographic modeling, and texture images. Descriptive statistics proved useful in summarizing pixel data from these images and converting them into quantifiable damage features suitable for Random Forest classification.

Correlation-based feature selection and Random Forest attribute ranking effectively reduced the number of predictor attributes thus enhancing model performance. Binary and ternary Random Forest models were developed using selected elevation and texture features. The best-performing models, R-A1 (completely damaged vs. undamaged), R-A2 (damaged vs. undamaged), and R-B1 (completely damaged, partially damaged, and undamaged), were identified based on evaluation metrics and classifier error analysis. This study highlighted the challenges in identifying and classifying building damage markers, some of which are unique to the Philippine setting, and demonstrated the value of UAV-based assessments for rapid and high-resolution damage evaluation. This methodology demonstrates the potential of integrating UAV data and remote sensing techniques for post- disaster damage assessment and can serve as a foundation for future advancements in this field.

For future work, it is highly recommended to increase the size and diversity of the dataset to improve the robustness and generalizability of the models. Incorporating additional roof material types and structures, as well as other damage indicators could enhance the models' predictive capabilities. Alternative techniques for handling imbalanced datasets, such as oversampling, or synthetic data generation, should also be explored. Another kind of feature selection method could be investigated to identify the most relevant predictors for building damage classification. Additionally, other candidate attributes not utilized in this study, particularly those relevant to classifying damage levels in buildings with corrugated metal sheets, may be included. It is further recommended to apply the methodology to other typhoon-affected areas to account for varied building typologies, construction materials, and environmental conditions, allowing assessment of its adaptability. UAV imagery should also be collected as soon as possible after the disaster, ideally within one week, to capture undisturbed damage indicators before cleanup or repairs begin. The three-month gap between Typhoon Haiyan and the UAV image acquisition in this study may have limited the visibility of moderate damage, highlighting the importance of rapid post-disaster data collection.

Acknowledgements

The authors thank Matthew Cua for providing the UAV images used in this study. This work was supported by the Engineering Research and Development for Technology (ERDT) program of the Department of Science and Technology–Science Education Institute (DOST-SEI).

References

Akhmadiya, A., Nabiyev, N., Moldamurat, K., Kismanova, A., Prmantayeva, B., Brimzhanova, S., 2022: Application of GLCM textural based method with Sentinel-1 radar remote sensing data for building damage assessment. *IEEE International Conference on Smart Information Systems and Technologies,* 1–5. doi.org/10.1109/SIST54437.2022.9945758.

Arun Kumar, C., Sooraj, M.P., Ramakrishnan, S., 2017: A comparative performance evaluation of supervised feature selection algorithms on microarray datasets. *Procedia Computer Science,* 115, 209–217. doi.org/10.1016/j.procs.2017.09.127.

Cooner, A.J., Shao, Y., Campbell, J.B., 2016: Detection of urban damage using remote sensing and machine learning algorithms: Revisiting the 2010 Haiti earthquake. *Remote Sensing,* 8(10), 868. doi.org/10.3390/rs8100868.

Dong, L., Shan, J., 2013: A comprehensive review of earthquake-induced building damage detection with remote sensing techniques. *ISPRS Journal of Photogrammetry and Remote Sensing,* 84, 85–99. doi.org/10.1016/j.isprsjprs.2013.06.011.

Everaerts, J., 2008: The use of unmanned aerial vehicles (UAVs) for remote sensing and mapping. *International Archives of the Photogrammetry Remote Sensing and Spatial Information Sciences,* XXXVII-B1, 1187–1192.

Gonsoroski, E., Ahn, Y., Harville, E.W., Countess, N., Lichtveld, M.Y., Pan, K., Beitsch, L., Sherchan, S.P., Uejio, C.K., 2023: Classifying building roof damage using high resolution imagery for disaster recovery. *Photogrammetric Engineering and Remote Sensing,* 89(7), 437-443. doi.org/10.14358/PERS.22-00106R2.

Hall, M., 1999: Correlation-based feature selection for machine learning. University of Waikato. cs.waikato.ac.nz/ml/publications/1999/99MH-Thesis.pdf (21 October 2025).

Joshi, A.R., Tarte, I., Suresh, S., Koolagudi, S.G., 2017: Damage identification and assessment using image processing on post-disaster satellite imagery. *IEEE Global Humanitarian Technology Conference,* 1–7. doi.org/10.1109/GHTC.2017.8239286.

Kerle, N., Nex, F., Gerke, M., Duarte, D., Vetrivel, A., 2020: UAV-based structural damage mapping: A review. *ISPRS International Journal of Geo-Information,* 9(1), 14. doi.org/10.3390/ijgi9010014.

Manzano, A.P.J., 2025: Post-disaster infrastructure damage assessment using 3D surface models derived from unmanned aerial vehicle (UAV) imagery. University of the Philippines Diliman. digitalarchives.upd.edu.ph/item/63190/9/ (6 February 2026).

Mathews, A.J., Singh, K.K., Cummings, A.R., Rogers, S.R., 2023: Fundamental practices for drone remote sensing research across disciplines. *Drone Systems and Applications,* 11, 1-22. doi.org/10.1139/dsa-2023-0021.

Menderes, A., Erener, A., Sarp, G., 2015: Automatic detection of damaged buildings after earthquake hazard by using remote sensing and information technologies. *Procedia Earth and Planetary Science,* 15, 257–262. doi.org/10.1016/j.proeps.2015.08.063.

Miura, H., Aridome, T., Matsuoka, M., 2020: Deep learning-based identification of collapsed, non-collapsed and blue tarp-covered buildings from post-disaster aerial images. *Remote Sensing,* 12(12), 1920. doi.org/10.3390/rs12121924.

NDRRMC, 2014: Final report re effects of Typhoon Yolanda ("Haiyan"). National Disaster Risk Reduction and Management Council. ndrrmc.gov.ph/attachments/article/1329/FINAL_REPORT_re_Effects_of_Typhoon_YOLANDA_HAIYAN_06-09NOV2013.pdf (30 January 2025).

Perante, W.C., 2016: Validity and reproducibility of typhoon damage estimates using satellite maps and images. *Asian Journal of Applied Science and Engineering,* 5(1), 105–116. doi.org/10.18034/ajase.v5i1.70.

Sonobe, M., 2020: Characteristics of texture index of damaged buildings using time-series high-resolution optical satellite images. *International Archives of the Photogrammetry, Remote Sensing and Spatial Information Sciences,* XLIII-B3-2020, 1709–1714. doi.org/10.5194/isprs-archives-XLIII-B3-2020-1709-2020.

Tu, J., Sui, H., Feng, W., Song, Z., 2016: Automatic building damage detection method using high-resolution remote sensing images and 3D GIS model. *ISPRS Annals of the Photogrammetry, Remote Sensing and Spatial Information Sciences,* III-8, 43–50. doi.org/10.5194/isprs-annals-III-8-43-2016.

Vetrivel, A., Gerke, M., Kerle, N., Vosselman, G., 2015: Identification of damage in buildings based on gaps in 3D point clouds from very high resolution oblique airborne images. *ISPRS Journal of Photogrammetry and Remote Sensing,* 105, 61–78. doi.org/10.1016/j.isprsjprs.2015.03.016.

Wen, H., Hu, J., Xiong, F., Zhang, C., Song, C., Zhou, X., 2023: A random forest model for seismic-damage buildings identification based on UAV images coupled with RFE and object-oriented methods. *Natural Hazards,* 119(3), 1751-1769. doi.org/10.1007/s11069-023-06186-5.

Womble, J.A., 2005: Remote-sensing applications to windstorm damage assessment. Texas Tech University. ttu-ir.tdl.org/items/be72f1e9-ede1-4507-9e3b-269d701434ba/full (30 January 2025).

Yeom, J., Han, Y., Chang, A., Jung, J., 2019: Hurricane building damage assessment using post-disaster UAV data. *IEEE International Geoscience and Remote Sensing Symposium,* 9867–9870. doi.org/10.1109/IGARSS.2019.8900477.

Appendix

<table>
<tr><th rowspan="2">PDA (%)</th><th rowspan="2">DR</th><th colspan="3">BINARY CLASS</th><th colspan="2">TERNARY CLASS</th></tr>
<tr><th>A1</th><th>A2</th><th>A3</th><th>B1</th><th>B2</th></tr>
<tr><td>0</td><td>0</td><td>UNDAMAGED</td><td>UNDAMAGED</td><td rowspan="2">UNDAMAGED</td><td>UNDAMAGED</td><td rowspan="2">UNDAMAGED</td></tr>
<tr><td>≤10</td><td>1</td><td rowspan="9">N/A</td><td rowspan="10">DAMAGED</td><td rowspan="9">PARTIALLY DAMAGED</td></tr>
<tr><td>≤20</td><td>2</td><td rowspan="9">DAMAGED</td><td rowspan="5">PARTIALLY DAMAGED</td></tr>
<tr><td>≤30</td><td>3</td></tr>
<tr><td>≤40</td><td>4</td></tr>
<tr><td>≤50</td><td>5</td></tr>
<tr><td>≤60</td><td>6</td></tr>
<tr><td>≤70</td><td>7</td><td rowspan="4">COMPLETELY DAMAGED</td></tr>
<tr><td>≤80</td><td>8</td></tr>
<tr><td>≤90</td><td>9</td></tr>
<tr><td>100</td><td>10</td><td>COMPLETELY DAMAGED</td><td>COMPLETELY DAMAGED</td></tr>
</table>

Table 1A. Damage rating and damage classification rules.

This contribution has been peer-reviewed. The double-blind peer-review was conducted on the basis of the full paper.
https://doi.org/10.5194/isprs-annals-X-5-W4-2025-331-2026 | © Author(s) 2026. CC BY 4.0 License.